JOURNAL OF GEOPHYSICAL RESEARCH, VOL. 104, NO. D10, PAGES 12,113–12,129, MAY 27, 1999

Correlation between smoke and tropospheric ozone concentration in Cuiabá during Smoke, Clouds, and Radiation-Brazil (SCAR-B)

Karla M. Longo,[1,2] Anne M. Thompson,[2] Volker W. J. H. Kirchhoff,[3] Lorraine A. Remer,[2] Saulo R. de Freitas,[1] Maria A. F. Silva Dias,[4] Paulo Artaxo,[1] William Hart,[2] James D. Spinhirne,[2] and Márcia A. Yamasoe[1]

Abstract. Ozone soundings launched from Cuiabá between August 16 and September 10, 1995, during the Smoke, Clouds, and Radiation–Brazil (SCAR-B) experiment show an enrichment of tropospheric ozone when compared with average wet season values and also present a great variability in concentrations depending on the dominant circulation pattern. Smoke tracers, such as aerosol optical thickness, measured from a Sun photometer installed at the Instituto Nacional de Pesquisas Espaciais-Cuiabá site, and black carbon ground measurements, also show an enhancement of smoke during the same period. Although there is a connection between the enrichment of the tropospheric ozone around Cuiabá during the dry season and smoke from biomass burning, the correlation between ozone and smoke indicates different behavior in different periods. Trajectory analyses suggest that the strong ozone peak measured in the period between August 26 and 29, 1995, may be associated not only with direct biomass-burning emissions but also with urban/industrial emissions from big cities on the coast of Brazil and recirculation of old smoke. This view is confirmed by measurements made from the Cloud Lidar System instrument aboard the ER-2 aircraft.

1. Introduction

In the Amazon and central Brazil regions during the austral winter dry season, between the months of July and October, intense anthropogenic biomass burning occurs in cerrado and tropical forest ecosystems [*Andreae*, 1991; *Crutzen and Goldammer*, 1993]. This biomass burning is a source of atmospheric pollution, emitting gases such as CO, CO_2, and NO_x; hydrocarbons; and aerosol particulates [*Crutzen et al.*, 1979; *Artaxo et al.*, 1994, 1997; *Echalar et al.*, 1998]. Also, gases that are not emitted directly from biomass burning but that result from secondary reactions of biomass-burning products, such as tropospheric ozone, show an enhancement in concentration during the biomass-burning season [*Kirchhoff et al.*, 1992, 1996a, b; *Thompson et al.*, 1996].

The overall objective of the Smoke, Clouds, and Radiation–Brazil (SCAR-B) experiment was to study the physical and chemical properties of the smoke produced by biomass burning and the effects of the smoke on the Earth's radiation balance and climate. Understanding the circulation pattern and the vertical structure of the atmosphere during the burning season is essential to interpreting and analyzing the measurements conducted during SCAR-B. Trajectory analyses based on a numerical simulation of the experiment period will be presented in this paper. Forward trajectories from the main fire areas and backward trajectories from the Cuiabá measurement site were calculated. The effects of meteorological conditions in spreading the pollutants emitted by biomass burning in Brazil are also discussed. The analyses presented in this paper are based on the daily variability of the ozone vertical profiles from ozonesondes launched at the Cuiabá site during the SCAR-B experiment. Origins of air parcels at Cuiabá at many vertical levels are examined. The daily variability of smoke tracers from ground-based measurements at the same site is also considered. Attention is given to the relationship between ozone, black carbon, and aerosol optical thickness. Different patterns of correlation, depending on the atmospheric circulation pattern, are investigated.

2. Methodology

2.1. Measurements at Cuiabá

During the SCAR-B experiment many measurements took place at the Cuiabá site, located in central Brazil (16°S, 56°W), where cerrado is the dominant vegetation, and many vegetation fires were observed. Ozonesondes were launched from Cuiabá in the manner described by *Kirchhoff et al.* [1992, 1996a, b]. The first measurement occurred on August 16, 1995, and the last one occurred on September 10, 1995; during this period a total of 20 ozonesondes were successfully launched.

A Sun photometer ground station installed at Instituto Nacional de Pesquisas Espaciais (INPE)-Cuiabá measured aerosol optical thickness during the same period. The aerosol optical thickness is the vertical optical thickness of the nonmolecular components of the entire atmospheric column derived from solar transmission measurements made by a Sun photometer [*Kaufman and Fraser*, 1983]. Precipitable water

[1]Instituto de Física, Universidade de São Paulo, São Paulo, Brazil.
[2]NASA Goddard Space Flight Center, Greenbelt, Maryland.
[3]Instituto Nacional de Pesquisas Espaciais, São José dos Campos, São Paulo, Brazil.
[4]Departamento de Ciências Atmosféricas, Instituto Astronômico e Geofísico, Universidade de São Paulo, São Paulo, Brazil.

Paper number 1999JD900044.
0148-0227/99/1999JD900044$09.00

vapor is retrieved from the same Sun photometer as the ratio of broad and narrow bands centered in the water vapor absorption region 0.935 to 0.950 μm [*Kaufman et al.*, 1992].

Real-time black carbon measurements were carried out using an aethalometer installed at INPE-Cuiabá with measuring intervals of 30 min. Black carbon includes all the particulate carbon species that efficiently absorb light [*Reid et al.*, 1998], which is abundantly emitted during biomass burning [*Echalar et al.*, 1998]. The data collected in this way represent a near-surface smoke measurement.

2.2. Trajectory Calculations

Kinematic three-dimensional trajectories were determined by the University of São Paulo (USP) Trajectory Model [*Freitas et al.*, 1996]. The wind fields used were generated from a simulation using the Regional Atmospheric Modeling System (RAMS), 3b version [*Tripoli and Cotton*, 1982]. The RAMS model was run with 80 km by 80 km grid resolution covering South America and neighboring Atlantic and Pacific Oceans. A stretched, terrain-following vertical coordinate was employed with a grid spacing of 200 m adjacent to the surface. Above 200 m the grid spacing gradually increases to 1200 m at a rate of 1.2, keeping this resolution up to the model top at 19 km. Physical parameterizations included in the RAMS model are anisotropic turbulence, which is dependent on the deformation tensor; atmospheric long- and short-wave radiation interacting with water vapor and liquid water; surface interaction including the effect of vegetation types; input from a soil model; and the effect of deep cumulus clouds. Details of these parameterizations are given by *Pielke et al.* [1992]. The RAMS simulations were carried out from an initial condition provided by an interpolation of six hourly National Center for Environmental Prediction (NCEP) global reanalyses, at 2.5 by 2.5 resolution, with 13 vertical levels from 1000 to 70 hPa. The model is nudged at every time step toward the NCEP analyses at the model boundary, at the model top, and significantly, but to a lesser extent, at the model center. In this way the simulation can be carried out for several days with the simulated wind fields reproducing large-scale features of the observed flow depicted in the NCEP analyses. The three-dimensional simulated winds are stored every 2 hours of simulation. These winds become input to the trajectory computation by the USP model, which uses a 0.5-hour time step.

The trajectories calculated using simulated wind fields as described before, rather than directly using NCEP winds, have the advantages of better time and spatial resolution. Also, the model takes into account surface effects, vegetation, and topography maps. These characteristics are particularly important while calculating trajectories inside the boundary layer.

3. Results

3.1. Meteorological Setting

The main large-scale systems affecting central Brazil and the Amazon Basin during the dry season in the Southern Hemisphere are the Intertropical Convergence Zone (ITCZ), the Midlatitude Frontal Systems, and the South Atlantic Subtropical High (SASH) [*Nobre et al.*, 1998]. The westward displacement of the SASH and the northward motion of the ITCZ during the austral winter typically produce a high-subsidence area over central Brazil and the Amazon Basin, displacing wetness and cloudiness to remote areas in the north and northwest Amazon.

Approaching cold frontal systems from the south are responsible for disturbances in atmospheric stability and in the wind fields. During these episodes, vertical advection is favored and so is long-range transport, although the cold frontal systems are usually blocked by the high-pressure system and are driven eastward to the Atlantic Ocean before they can reach the SCAR-B area [*Freitas et al.*, 1996]. These disturbances contribute to the daily variability of air mass origins and of ozone vertical profiles at Cuiabá during SCAR-B. From the north, propagating squall lines originating at the northern coast of Brazil can also be responsible for convective events [*Silva Dias and Ferreira*, 1992]. During the 1992 Transport and Atmospheric Chemistry Near the Equator—Atlantic (TRACE-A) experiment, convective events were observed, related to both the approach of a cold frontal system and northern convection [*Pickering et al.*, 1996].

During the SCAR-B experiment period, from August 16 to September 11, 1995, a high-pressure area with very little precipitation dominated the central Brazil climatology. Moderate to slow easterly winds were observed above 15°S latitude, where most of the biomass burning took place. Also, winds came from the north and northwest of the SCAR-B area. This anticyclonic circulation over the continent pushed the smoke southward toward the cold frontal system, where the smoke was strongly advected upward, with injection at high levels and transport to the South Atlantic Ocean by the westerly winds. Figure 1 shows the time-averaged wind fields for the SCAR-B period. *Pickering et al.* [1996] and *Wang et al.* [1996] have described this type of behavior and its chemical impact during TRACE A.

At the Cuiabá site, where the data collection took place, easterly winds are dominant, bringing clean air from the ocean and some recirculation from the continent. In some periods, depending on the anticyclonic position, north or northeast winds were also observed at Cuiabá.

3.2. Trajectory Analysis

Although ozone is not emitted directly from biomass burning, an enhancement of tropospheric ozone has been reported for periods of biomass burning in Brazil and Africa [*Kirchhoff et al.*, 1992, 1996a; *Fishman et al.*, 1996; *Thompson et al.*, 1996; *Browell et al.*, 1996; *Jacob et al.*, 1996]. The TRACE-A measurements conducted over the tropical South Atlantic Ocean indicated that widespread biomass burning over both South America and Africa was a dominant source of precursor gases necessary for formation of the large amount of ozone over the Atlantic Ocean [*Thompson et al.*, 1996]. Case studies from several experiments over South America and the tropical Atlantic have shown that the seasonal increase in free tropospheric ozone formation is frequently associated with the combination of deep convection and biomass-burning pollution or urban emissions [*Thompson et al.*, 1997; *Jenkins et al.*, 1997].

During the 1995 dry season, GOES 8 smoke observation data from University of Wisconsin–Madison (UW–Madison) showed an extensive smoke layer over Brazil, almost entirely covering the Amazon Basin and heading southward toward continental outflow to the Atlantic Ocean [*Prins et al.*, 1998]. Forward trajectories from the main fire areas in Brazil calculated for the period of SCAR-B present a good fit with these smoke observations.

Plate 1 shows hourly parcel positions distributed along 6-day forward trajectories for the SCAR-B period. These trajectories originated from the main biomass areas during SCAR-B, as

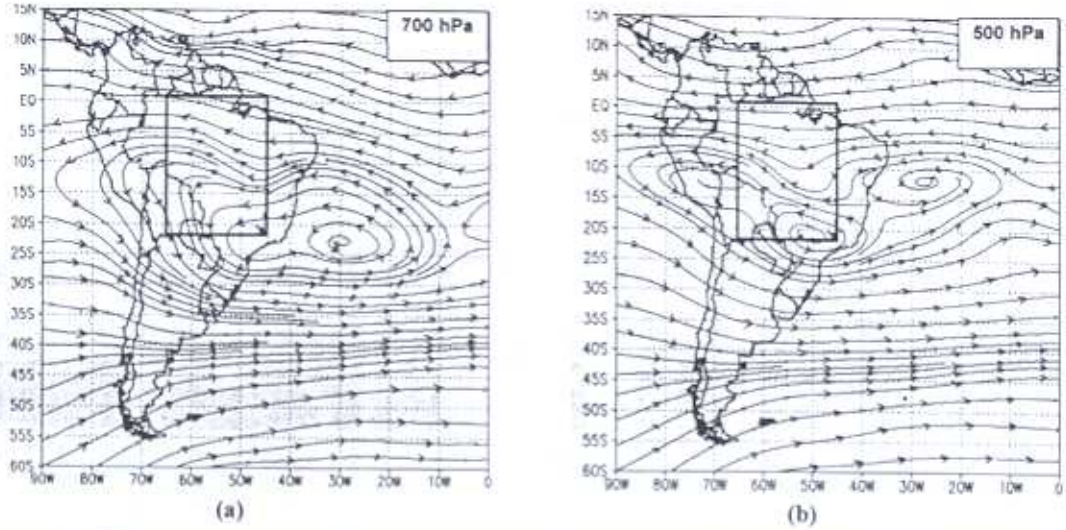

Figure 1. Time-averaged wind fields (streamlines) for the SCAR-B period, August 16 to September 11, 1995, derived from four daily (0000, 0600, 1200, and 1800 UTC) National Center for Environmental Prediction (NCEP) global reanalyses at (a) 700 hPa and (b) 500 hPa.

observed by the GOES 8 fire product data from UW–Madison [*Prins et al.*, 1998]. Three areas were considered relevant (white rectangles in Plate 1). The first area (Plate 1a) is in Rondônia, southeast of Porto Velho (from 7.5°S to 15°S and 65°W to 60°W). The second area (Plate 1b) surrounds the town of Alta Floresta in northern Mato Grosso (from 7.5°S to 12.5°S and 60°W to 52.5°W). Finally, the third area (Plate 1c) is northwest of Porto Nacional (from 5.0°S to 12.5°S and 52.5°W to 47.5°W). These trajectories were initialized at ~700 hPa (~3 km). According to meteorological observations from the National Institute of Meteorology in Brazil an inversion layer at ~700 hPa over central Brazil was observed at several meteorological sites during nearly all of the SCAR-B period. Also, many smoke tracer layers observed during vertical profiling aboard INPE aircraft suggest the same altitude for the inversion layer.

The Porto Velho area receives pollution from the other areas in addition to the local pollution effects (Plate 1a). The Sun photometers installed at Porto Velho, Ji-Paraná, and Potosí Mine indicated high values of aerosol optical thickness, rarely below 2.0 for the 0.669 μm channel. The dominant easterly winds push the smoke toward the Andes, and high subsidence maintains the smoke at low levels for several days. The trajectory altitudes remain below 700 hPa (3.0 km) while inside the Amazon Basin. Plotting air parcel distributions along the forward trajectories originating from the three main areas (Plate 1d) shows a plume over Brazil with continental outflow to the Atlantic Ocean ~30°S latitude. A stationary cold front at 30°S latitude is responsible for a strong vertical motion at this point. The trajectory altitudes jump to values >6.0 km upon reaching the cold front area, indicating the possibility of long-range transport of the biomass-burning products. Outflow to the Pacific Ocean across the Andes is also indicated between the latitudes 10°S and 10°N. The low levels of the trajectories, however, could indicate an important deposition effect, mainly considering that even during the dry season the northern portion of the Amazon Basin may still possess high relative humidity. During August 1995 the observed precipitation levels in the extreme north of the Amazon Basin (Roraima and northwestern Amazonas) exceeded 200 mm [*Instituto Nacional de Pesquisas Espaciais* (*INPE*), 1995].

Plate 2 shows two illustrative clusters of the 6-day forward trajectories for particular days in order to exemplify two basic patterns of the period as a whole. The first one ends on August 29, 1995, and the second one ends on September 4, 1995. The color bar in Plate 2 indicates the altitude of the air parcels along the integration. During high-subsidence periods (Plate 2a) the absence of the trajectory vertical motion indicates that the smoke is trapped below 700 hPa while in central Brazil. There is an upward movement ahead of the cold frontal system in southern Brazil and also associated with convective systems in the northern Amazon Basin. The second cluster (Plate 2b) shows an example where the trajectory upward motion is substantial owing to convective events that are smaller in scale than cold frontal systems but still sensitive to the model.

This transport pattern results in a large smoke layer as indicated in Plate 1d and confirmed by satellite smoke observation [*Prins et al.*, 1998; *Gleason et al.*, 1998]. Thus the effects of these emissions exceed the local scale and may affect the regional composition of the South American atmosphere. These biomass-burning emissions may change the atmospheric radiative balance and the hydrological cycle by direct effects of the aerosol particulate and gases as well as by indirect effects on dynamics of the cloud formation [*Kaufman*, 1995; *Kaufman et al.*, 1998].

Hourly parcel positions along 6-day backward trajectories originating from the Cuiabá site at 700 hPa during SCAR-B are summarized in Plate 3. Easterly winds bring clean air from the ocean and some recirculation from the continent.

3.3. Ozonesondes

Ozone concentration mean values ranging from 40 to 90 ppbv were observed from August 16 to September 10 (Figure 2). From August 16 to 25 the ozone levels observed in Cuiabá were relatively low, ~50 ppbv. These values are still high when compared with typical wet season values (~15 ppbv). An increase of tropospheric ozone was observed, starting on August 26 and reaching a maximum on August 29; ozone decreased again at the beginning of September. During the first 10 days of September, alternating periods of high- and low-ozone con-

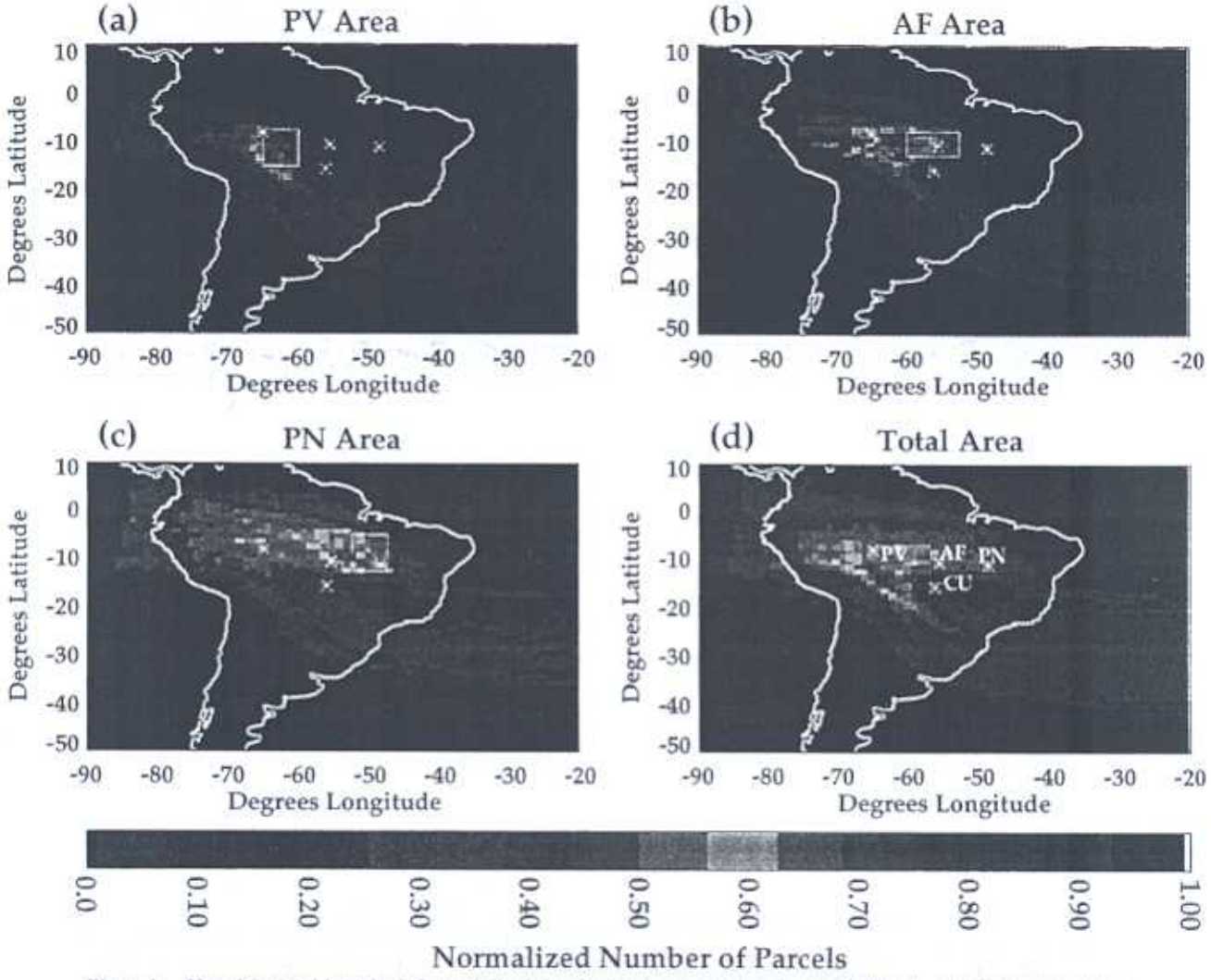

Plate 1. Hourly parcel locations from daily 6-day forward trajectories during SCAR-B, originating from the main biomass-burning areas at 700 hPa. Three source areas, (a) Rondônia, (b) northern Mato Grosso, around the town of Alta Floresta, and (c) an area including southeastern Pará, western Tocantins, and northeastern Mato Grosso, were considered as well as (d) all three source areas together. PV, Porto Velho; AF, Alta Floresta; PN, Porto Nacional.

centrations were recorded, with values higher than those observed before August 26.

Vertical ozone, relative humidity, and temperature profiles available for two particular periods are plotted in Figures 3 and 4. Period 1 is from August 26 to 31, and period 2 is from September 7 to 10.

On August 26 (Figure 3a), ozone levels start rising and begin forming a layer at 700 hPa; also, two smaller peaks are observed at 650 and 550 hPa. On August 27 (Figure 3b), there was a 100 ppbv ozone layer above 700 hPa and a clean gap between it and a weaker layer at lower levels. On August 29 a narrow plume of 140 ppbv was registered ~650 hPa (Figure 3c). Figure 3d shows the ozone decreasing on August 31.

Vertical profiles for period 2 present a different vertical structure (Figure 4). The period from September 7 to 10 is characterized by a transition phase from the dry to the wet season. The high-pressure area over central Brazil has dispersed, promoting a stratified vertical structure of the atmosphere. The boundary layer is much more flexible, allowing greater upward motion and expanding the ozone layer up to 500 hPa with a maximum concentration at 700 hPa.

3.4. Aerosol Optical Thickness and Aethalometer Results

The smoke tracers show a pattern of daily variability in the SCAR-B period from August 16 to September 10 similar to the variation in ozone. Relatively low levels in the first week of measurement (August 16–23) and an enhancement around August 29 were observed. Figure 5 presents daily averages for the black carbon ground measurements, aerosol optical thickness, (0.669 μm channel), and precipitable water vapor.

The black carbon concentration in Cuiabá exhibits a diurnal cycle, with lower concentrations and variability between 1200 and 1800 UTC. Figure 6 shows an average day, including all the measurements collected at the indicated times between August 16 and September 10. The black carbon diurnal cycle is related to the fire diurnal cycle reported by the GOES 8 fire

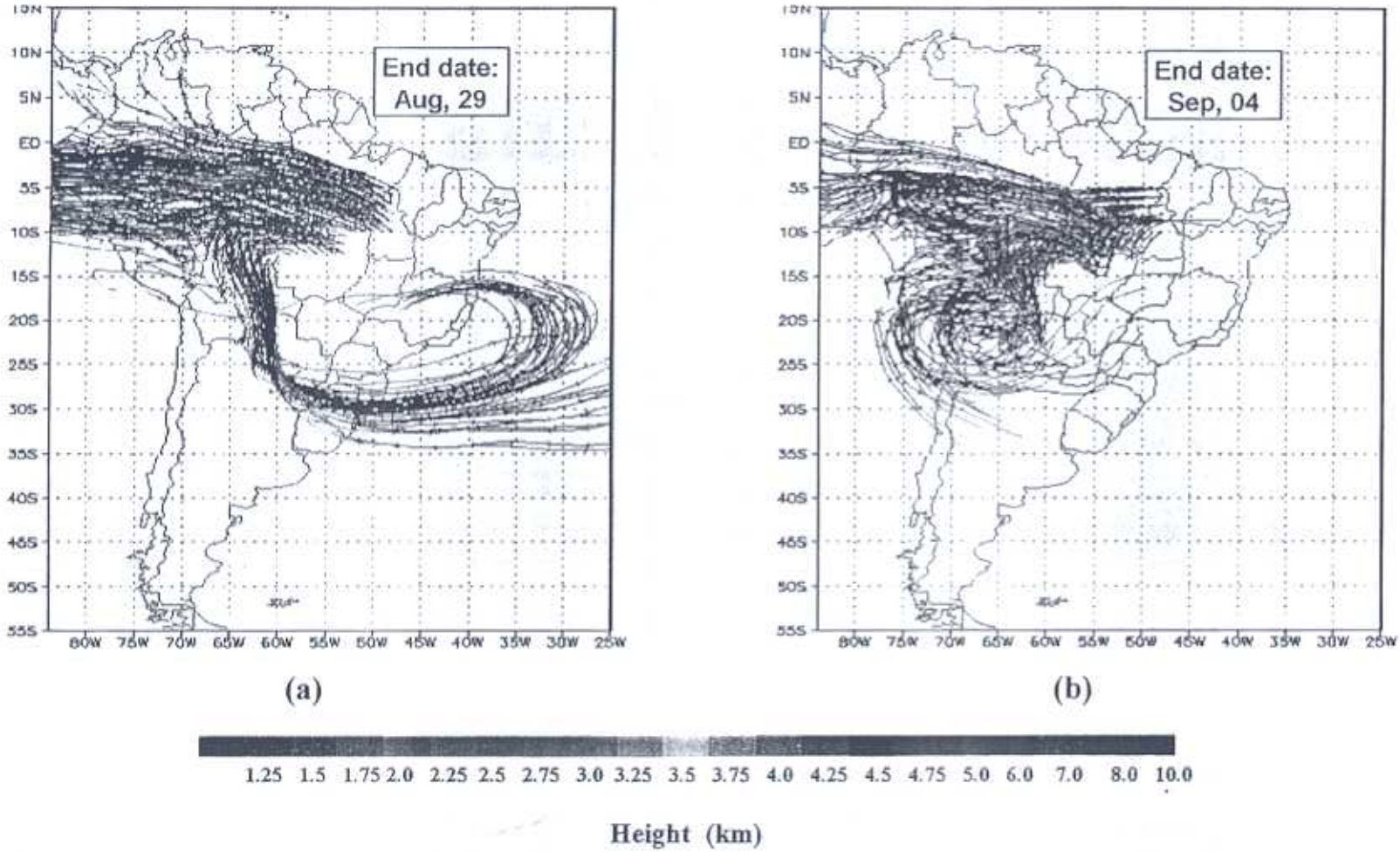

Plate 2. Clusters of 6-day forward trajectories originating from the main fire areas (described in Plate 1) at 700 hPa. Integration period is from (a) August 22 to 29 and (b) August 28 to September 4. The color bar gives the trajectory altitude.

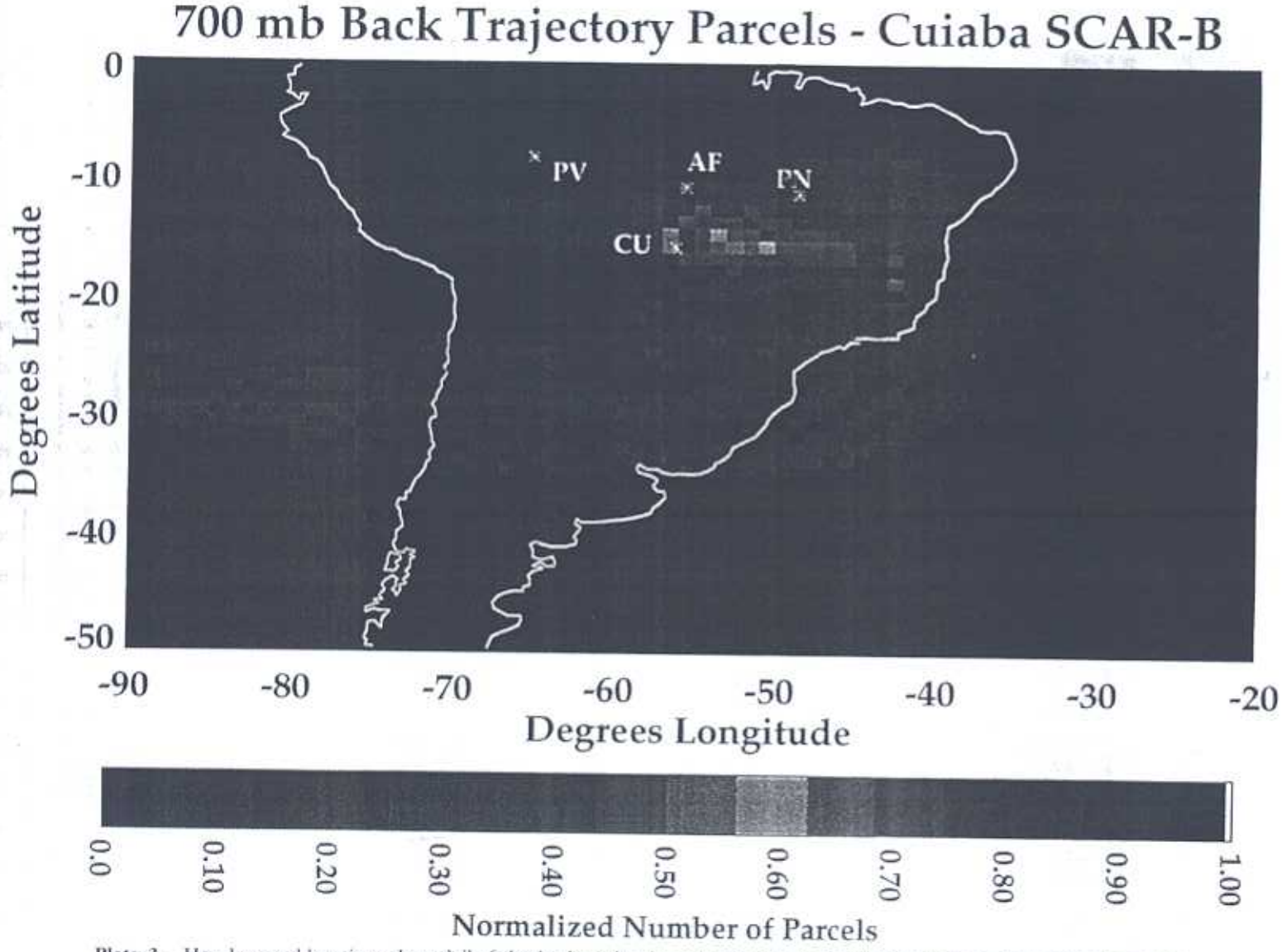

Plate 3. Hourly parcel locations along daily 6-day backward trajectories during the SCAR-B period. Trajectory starting points are distributed in a cluster around the Cuiabá site (16°S, 56°W), and starting levels are ~700 hPa.

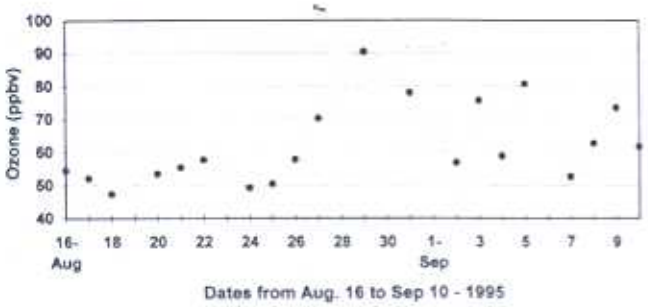

Figure 2. Average ozone concentrations from 1000 to 500 hPa, derived from the ozone profiles obtained from the ozonesonde measurements made at Cuiabá between August 16 and September 10, 1995.

products by UW–Madison. The fire count around 1745 UTC is typically 2–4 times greater than that observed three hours earlier or later and nearly 20 times greater than that observed at 1145 UTC [*Prins et al.*, 1998]. The black carbon diurnal cycle is also related to the boundary layer evolution during a diurnal cycle. The formation of the nocturnal boundary layer, as a result of contact of the first atmospheric layer with the ground, reduces the vertical upward motion of the pollutants [*Stull*, 1988], promoting smoke accumulation after sunset. Daily averages of black carbon that include only measurements taken between 1200 and 1800 UTC probably represent surface measurements in a well-mixed column. In the correlation graphs of smoke tracers and ozone described in section 3.5, only tracer data collected between 1200 and 1800 UTC will be considered.

3.5. Correlation Between Observed Parameters

The relationship between tropospheric ozone concentration and smoke in Cuiabá, as circulation patterns vary, will be explored here. Our analysis focuses on the two periods of enhancement of both ozone and smoke: from August 26 to 31 (period 1) and from September 7 to 10 (period 2). Black carbon (Figure 7a) and precipitable water vapor (Figure 7b) as functions of aerosol optical thickness (measured in the 0.669 μm channel) show a relationship in both cases. For high values of aerosol optical thickness (>0.5) a split pattern is observed. Period 1 (solid diamonds) shows higher values of black carbon (BC) and lower values of precipitable water vapor than period 2 (crosses) for the same range of aerosol optical thickness (AOT). Figure 8 shows the average tropospheric ozone, weighted by altitude from 1000 to 500 hPa, as a function of the aerosol optical thickness, measured simultaneously with the ozone data point. The ozone versus aerosol optical thickness repeats the same split pattern observed for black carbon and water vapor. In period 1 the atmosphere presents an enhancement of ozone concentration relative to period 2. The r^2 for the correlation of ozone as a function of AOT and BC as a function of AOT, excluding the last days of September, which characterize the transition from the dry to the wet season, were 0.74 and 0.63, respectively.

Note that lower ozone mixing ratios correspond to a higher presence of water vapor. This fits in with other observations of

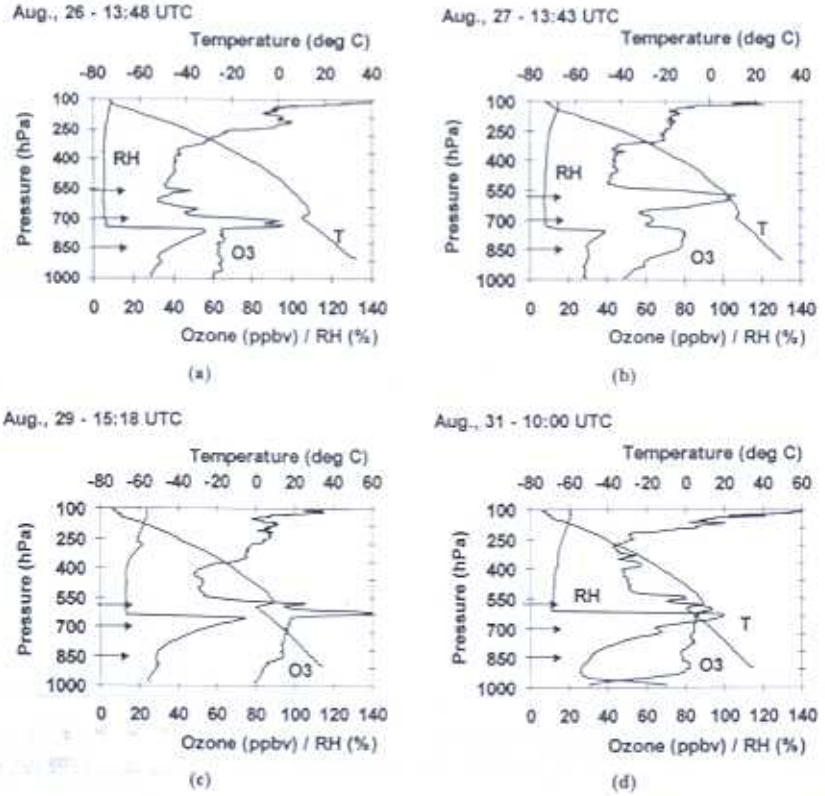

Figure 3. Radiosonde measurements of ozone (ppbv), relative humidity (%), and temperature (°C) at Cuiabá for period 1: (a) August 26, (b) August 27, (c) August 29, and (d) August 31. Shaded arrows indicate the levels from which the backward trajectories were calculated. Launch dates and times are shown above each plot.

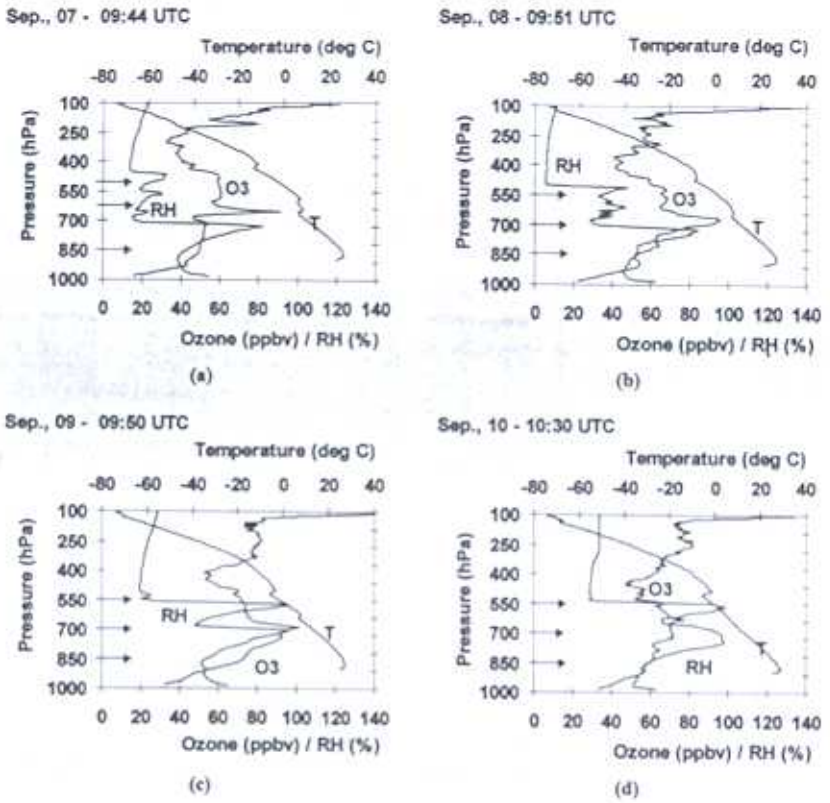

Figure 4. Radiosonde measurements of ozone (ppbv), relative humidity (%), and temperature (°C) at Cuiabá for period 2: (a) September 7, (b) September 8, (c) September 9, and (d) September 10. Shaded arrows indicate the levels where the backward trajectories were calculated. The launch dates and times are shown above each plot.

middle and lower-tropospheric anticorrelation of tropical water vapor and ozone [*Kley et al.*, 1996]. A main reason is that the photochemical destruction of ozone leads to the formation of the $O(^1D)$ free radical which reacts with water vapor to form the hydroxyl radical OH:

$$O_3 + h\upsilon \rightarrow O(^1D) + O_2$$

$$O(^1D) + H_2O \rightarrow OH + OH$$

This is the major loss process for tropospheric ozone in the lower atmosphere. The greater the amount of water vapor, the greater the ozone loss, and the lower the ozone concentration [*Thompson*, 1994].

Backward trajectories from Cuiabá measurement site are run at many levels in order to see if the origin of the air masses can explain the ozone changes and the different correlation patterns for different periods (Plate 4). Shaded arrows along the vertical profiles indicate vertical starting levels for these trajectories. Starting date and time are indicated at the top of the graphs. Starting vertical levels and the ending levels after 6 days for the trajectories in the center of each cluster are also shown in Plate 4. The color bar indicates the trajectory altitudes in kilometers. On August 26 and 27 the backward tra-

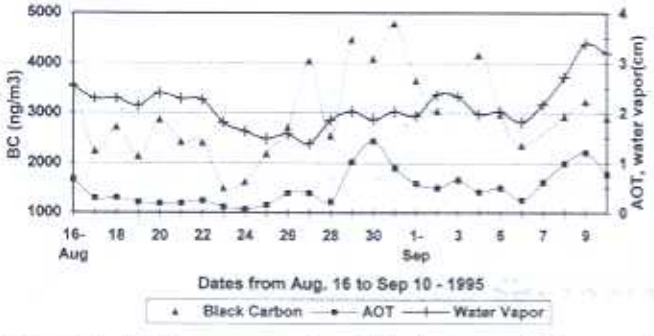

Figure 5. Daily average series of black carbon (BC) ground measurements (triangles), aerosol optical thickness (AOT) (rectangles) for 0.669 μm channel, and precipitable water vapor (pluses). The averages consider measurements taken between 1200 and 1800 UTC.

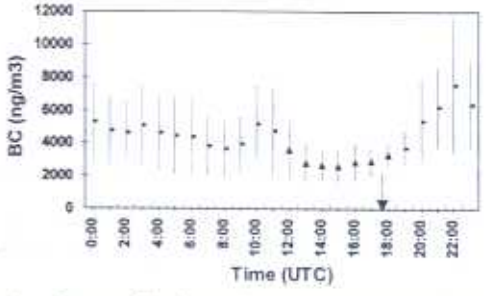

Figure 6. Average black carbon concentration (bars, standard deviation) for an "average day" between August 16 and September 10. The triangles indicate the times with lower concentrations and variability. The solid arrow indicates the peak burning reported by *Prins et al.* [1998].

jectories are eastward on the first 2 days of integration; after this the trajectories show an anticyclonic circulation from the continent. On August 29 the pattern is similar but with a component from the northeast on the first 3 days at 700 hPa. The aerosol optical thickness measured in Brasília (48.5°W, 15.5°S) in the August 26–29 period was always <0.1 (0.669 μm channel). In some levels, circulation is over the coast, overpassing an urban/industrial area; otherwise, the circulation is over the ocean. In both cases, air parcels reached the biomass-burning outflow region, at ~30°S latitude in this period. This circulation suggests that the ozone enhancement observed in Cuiabá during this period could be a superposition of ozone production from the local biomass-burning emissions trapped in an inversion brought on by very high subsidence and a postconvective production of ozone from vertically transported NO or NO produced by lightning [*Thompson et al.*, 1996; *Lelieveld and Crutzen*, 1990, 1994]. In addition, recirculation of the regional plume that covers part of Brazil during the burning season is probably introducing additional contributions of ozone from urban/industrial areas.

Vertical profiles from the radiosondes for period 2 present a different vertical structure (Figure 4). The period from September 7 to 10 is characterized by a transition phase from the dry to the wet season. The high-pressure area over central Brazil has dispersed, promoting a stratified vertical structure of the atmosphere. The boundary layer is much more flexible, allowing greater upward motion and expanding the ozone layer up to 500 hPa with a maximum concentration at 700 hPa. Backward trajectories for this period are shown in Plate 5, characterizing a more localized pattern of circulation, indicating slow air parcels predominantly from the northeast.

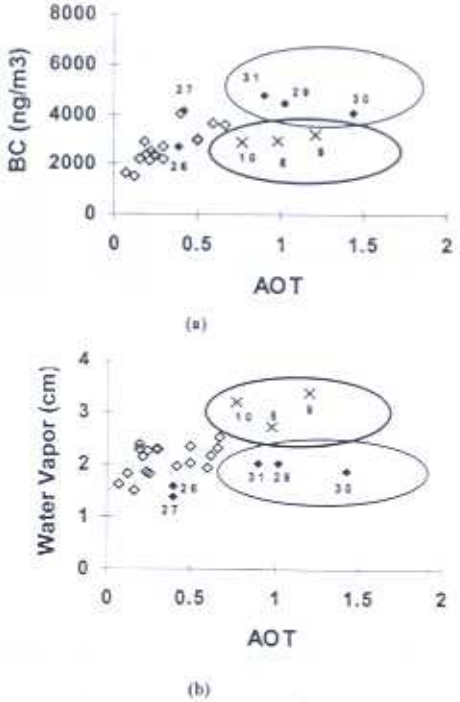

Figure 7. (a) Black carbon ground measurement and (b) precipitable water vapor as functions of aerosol optical thickness (0.669 μm). The open diamonds are for general days. The solid diamonds, inside the thin ellipses, indicate the days when the AOT increased owing to smoke accumulation during a very high subsidence period. The days where the increase of AOT corresponds to an increase of water vapor are represented by crosses inside the thick ellipses.

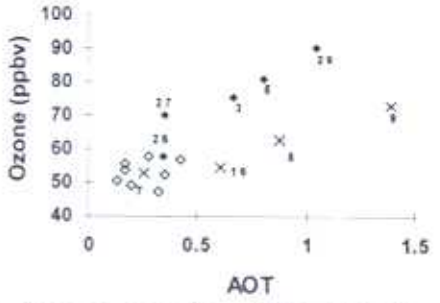

Figure 8. Average ozone (from 1000 to 500 hPa) as function of the aerosol optical thickness (0.669 μm). The same split pattern for black carbon and water vapor (Figure 7) repeats for the ozone.

3.6. Supporting Evidence: ER-2 Cloud Lidar System

A Nd:(yttrium/aluminium/garnet (laser crystal)) YAG monostatic lidar system aboard the ER-2 aircraft (the Cloud Lidar System (CLS)) measured the backscattered signals at 1.064 and 0.532 μm [*Spinhirne et al.*, 1982] during SCAR-B. Flights 95165 and 95169 refer to flights from Cuiabá to Vilhena on August 27 and September 7, respectively (Plate 6). On August 27, ozone concentrations from 50 to 80 ppbv were observed below the inversion layer ~700 hPa (~3.0 km). A second, stronger ozone layer, with ozone concentration of 100 ppbv, was observed ~600 hPa (~4.5 km) (Figure 3b). According to the lidar data this second ozone layer is not correlated with smoke. The aerosol backscatter coefficient derived from CLS on August 27 (Plate 6a) shows the smoke limited to the column below 3 km, trapped by the temperature inversion. Plate 4a shows the ozone profile with ozone concentrations from 40 to 60 ppbv from the surface to 500 hPa and a strong and thin ozone layer (~95 ppbv) at 600 hPa corresponding to a double temperature inversion. For the September 7 flight (Plate 6b) the CLS shows the smoke also in higher levels, coexisting with the ozone layer.

The CLS observations are consistent with the backward trajectory patterns for the two periods. Smoke recirculation with possible urban/industrial contributions pertains to period 1, whereas period 2 corresponds to a more localized circulation pattern, indicating local, fresh smoke.

4. Conclusions

A correlation between tropospheric ozone concentration and aerosol optical thickness was observed at Cuiabá during SCAR-B. Higher ozone concentrations were observed for days with lower values of water vapor. Aerosol optical thickness showed a relationship with black carbon and precipitable water vapor based on measurements taken during a period when fresh smoke plumes were not dominant. These correlations are dependent on the dominant circulation pattern. All correlation graphs present a split pattern for high values of aerosol optical thickness (>0.5, 0.669 μm channel). Comparing two high ozone and smoke episodes, it was observed that in the last week of August the increase of aerosol optical thickness corresponds to black carbon concentrations higher than observed for September 7 to 10. Conversely, the precipitable water vapor values are lower for the last week of August than for the

6 Day Backward Trajectories from Cuiabá

August 26 1995 - 14 UTC

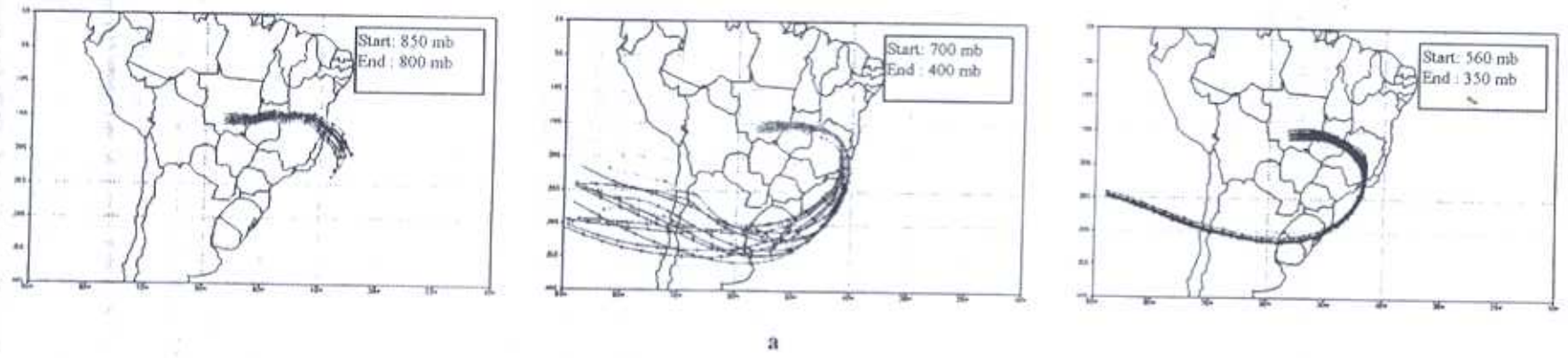

a

August 27 1995 - 14 UTC

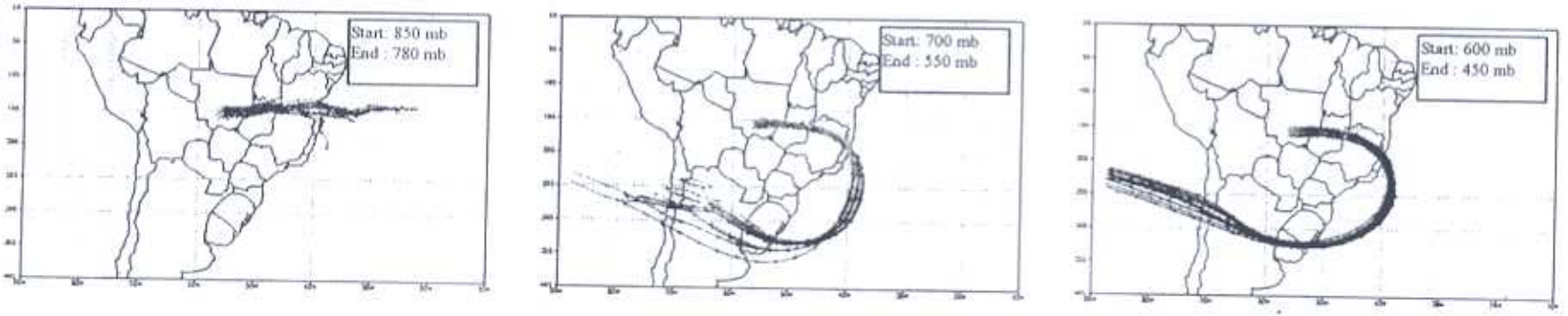

b

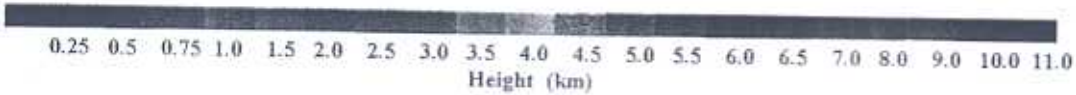

Plate 4. Six-day backward trajectories from Cuiabá starting on (a) August 26, (b) August 27, (c) August 29 and (d) August 31. Shaded arrows indicate the starting levels on the ozonesonde plots for these days (Figure 3). The trajectory starting dates and times are shown above the maps. The approximate trajectory start and end pressure levels are indicated.

6 Day Backward Trajectories from Cuiabá

August 29 1995 - 16 UTC

c

August 31 1995 - 14 UTC

d

Plate 4. (continued)

6 Day Backward Trajectories from Cuiabá

September 07 1995 - 16 UTC

a

September 08 1995 - 14 UTC

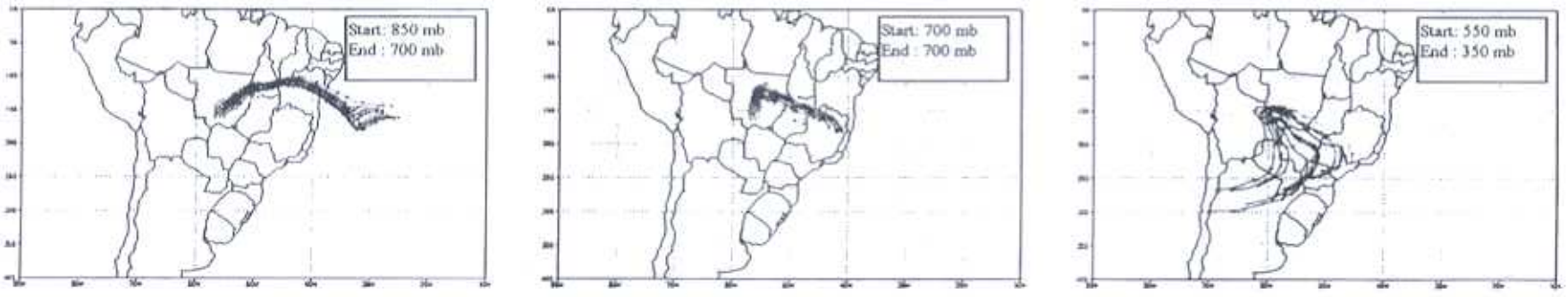

b

Plate 5. Six-day backward trajectories from Cuiabá starting on (a) September 7, (b) September 8, (c) September 9, and (d) September 10. Shaded arrows indicate the starting levels on the ozonesondes plots for these days (Figure 4). The trajectory starting dates and times are shown above the maps. The approximate trajectory start and end pressure levels are indicated.

6 Day Backward Trajectories from Cuiabá

September 09 1995 - 10 UTC

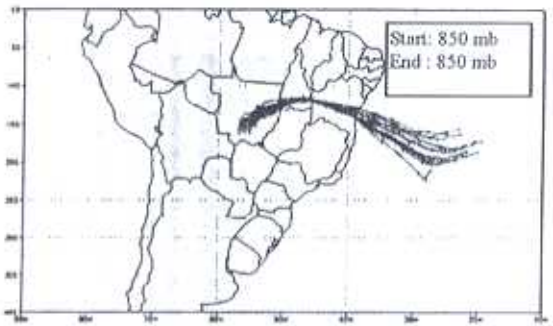

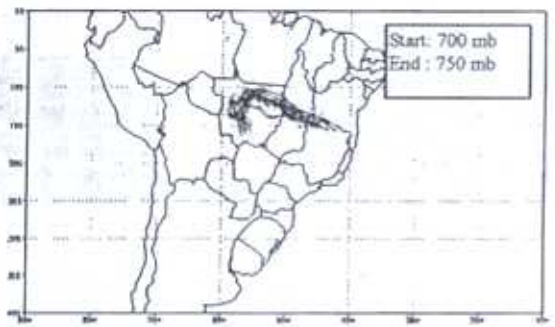

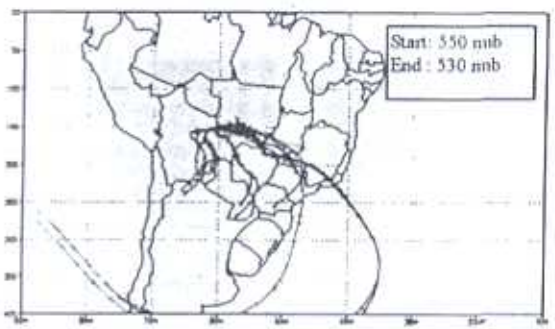

c

September 10 1995 - 10 UTC

d

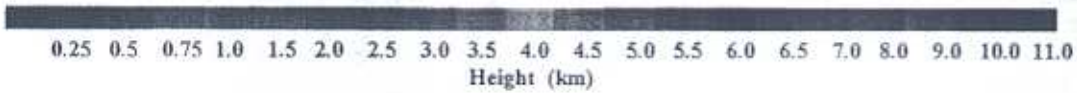

Plate 5. (continued)

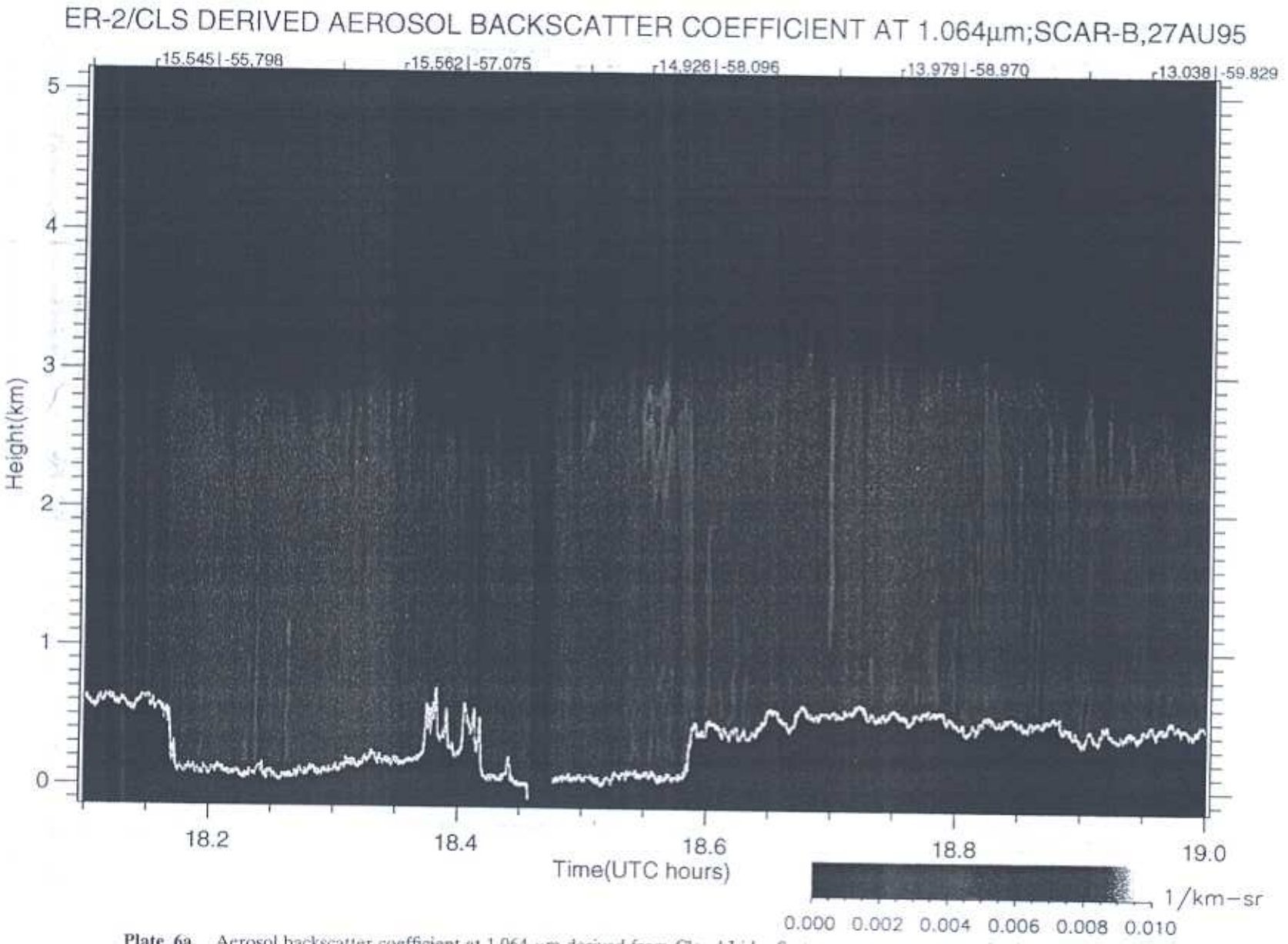

Plate 6a. Aerosol backscatter coefficient at 1.064 μm derived from Cloud Lidar System measurements made aboard ER-2 on flight 95165 on August 27 between Cuiabá and Vilhena. Latitude and longitude are given along the top, and measurement time is given along the bottom.

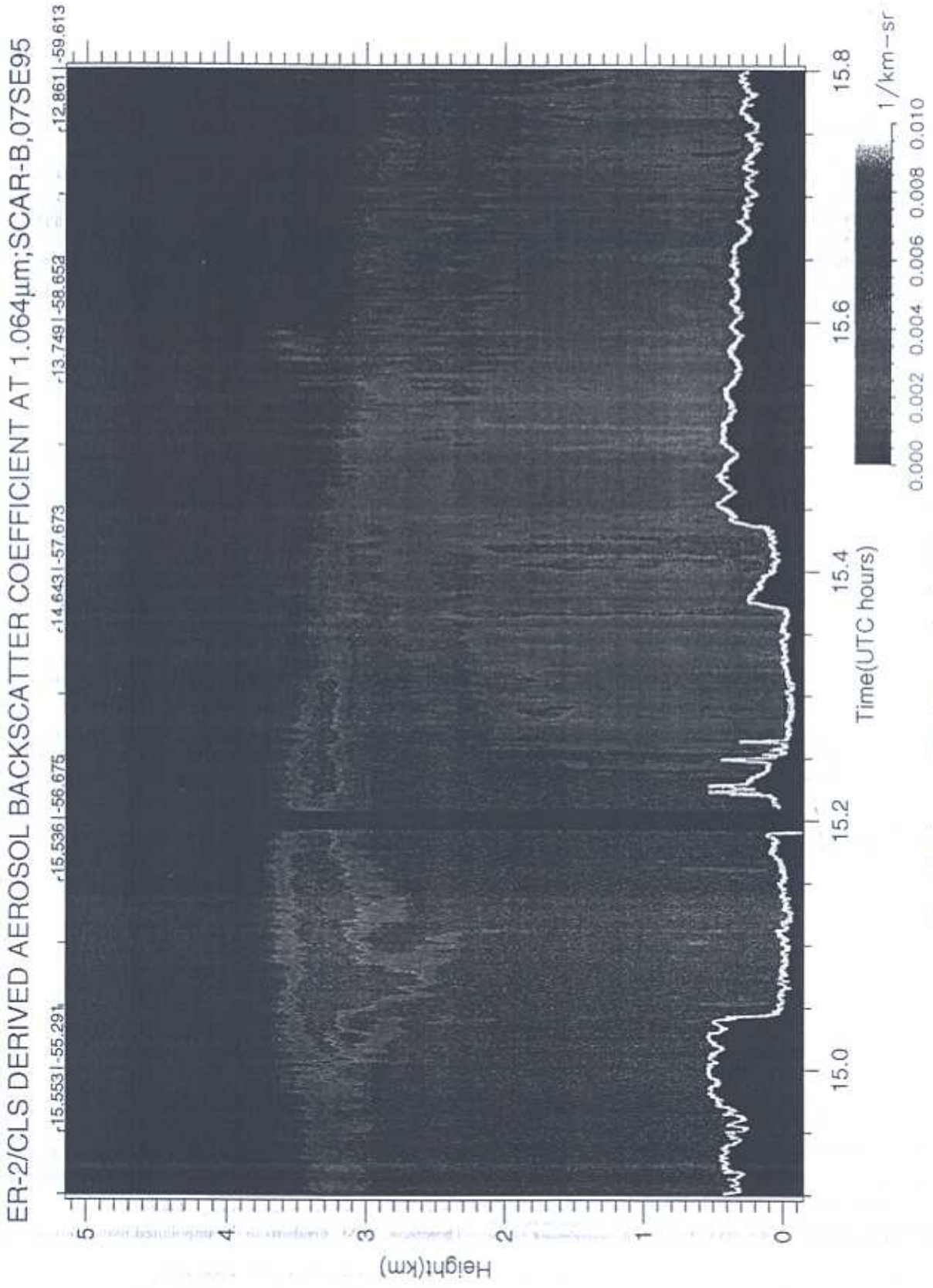

Plate 6b. Same as Plate 6a, except for flight 95169 on September 7.

September period. This is in agreement with the higher levels of ozone observed for the August period. Backward trajectory analyses from Cuiabá suggest that the ozone enhancement observed in the last week of August could be a superposition of two factors: (1) local emissions from biomass burning trapped in an inversion during a very high subsidence period and (2) recirculation of the regional plume that covers part of Brazil during the burning season plus a probable contribution of urban/industrial emissions. Comparison of the ER-2 CLS data and the ozone profile confirms the existence of an ozone layer not correlated with smoke, indicating the ozone long-distance transport during the August period.

The smoke outflow to the Atlantic Ocean and the occasional recirculation back to the continent is a cloud-related process, probably involving high precipitation rates and consequent smoke scavenging, including NO_x deposition (via the soluble nitric acid). Along the coast of Brazil at latitude 25°S, precipitation amounts >100 mm were observed during August 1995 [*INPE*, 1995]. The ozone layer formed by recirculation of old smoke and urban/industrial pollution, which is not correlated directly with aerosols, could be due to two different factors: (1) considerable ozone production while the smoke is still trapped in central Brazil and (2) a postconvective production of ozone from vertically transported NO produced by lightning [*Thompson et al.*, 1996; *Lelieveld and Crutzen*, 1990, 1994].

Acknowledgments. We would like to acknowledge E. Prins, University of Wisconsin–Madison, for processing and analyzing the GOES 8 fire products and NCEP for the large-scale data. Aster, Inc. licenses the RAMS code. This research is part of the first author's Ph.D. dissertation, which has been supported by CNPq and CAPES-PICD program. Thanks to USRA for additional support during the first author's NASA Goddard visit.

References

Andreae, M. O., Biomass burning: Its history, use and distribution and its impact on environmental quality and global climate, in *Global Biomass Burning: Atmospheric, Climatic and Biospheric Implications*, edited by J. S. Levine, pp. 3–21, MIT Press, Cambridge, Mass., 1991.

Artaxo, P., F. Gerab, M. A. Yamasoe, and J. V. Martins, Fine mode aerosol composition in three long-term atmospheric monitoring sampling stations in the Amazon Basin, *J. Geophys. Res.*, *99*, 22,857–22,868, 1994.

Artaxo, P., F. Gerab, and M. A. Yamasoe, Long term atmospheric aerosol characterization in the Amazon Basin, in *Environmental Geochemistry in the Tropics*, edited by J. Wasserman, E. V. Silva Filho, and R. Villas Boas, pp. 227–250, Springer-Verlag, New York, 1997.

Browell, E. V., et al., Ozone and aerosol distribution and air mass characteristics over the South Atlantic Basin during the burning season, *J. Geophys. Res.*, *101*, 24,043–24,068, 1996.

Crutzen, P. J., and J. G. Goldammer (Eds.), *Fire in the Environment: The Ecological, Atmospheric and Climate Importance of Vegetation Fires*, John Wiley, New York, 1993.

Crutzen, P. J., L. E. Heidt, J. P. Krasnec, W. H. Pollock, and W. Seiler, Biomass burning as a source of the atmospheric gases CO, H_2, N_2O, NO, CH_3Cl and COS, *Nature*, *282*, 253–256, 1979.

Echalar, F., P. Artaxo, J. V. Martins, M. A. Yamasoe, F. Gerab, W. Maenhaut, and B. Holben, Long-term monitoring of atmospheric aerosols in the Amazon Basin: Source identification and apportionment, *J. Geophys. Res.*, *103*, 31,849–31,864, 1998.

Fishman, J., J. M. Hoell Jr., R. D. Bendura, R. J. McNeal, and V. W. J. H. Kirchhoff, NASA GTE TRACE-A experiment (September–October 1992): Overview, *J. Geophys. Res.*, *101*, 23,865–23,879, 1996.

Freitas, S. R., K. M. Longo, M. A. F. Silva Dias, and P. Artaxo, Numerical modeling of air mass trajectories from the burning areas of the Amazon Basin, *An. Acad. Bras. Cienc.*, *68*, suppl. 1, 193–206, 1996.

Gleason, J., N. C. Hsu, and O. Torres, Biomass-burning smoke measured using backscattered ultraviolet radiation: SCAR-B and Brazilian smoke interannual variability, *J. Geophys. Res.*, *103*, 31,969–31,978, 1998.

Instituto Nacional de Pesquisas Espaciais (INPE), *Climanálise: Boletim de Monitoramento e Análise Climática*, Vol. 10, no. 8, São Jose dos Campos, Sao Paulo, Brazil, Aug. 1995.

Jacob, D. J., et al., Origin of ozone and NO_x in the tropical troposphere: A photochemical analysis of aircraft observations over the South Atlantic Basin, *J. Geophys. Res.*, *101*, 24,235–24,250, 1996.

Jenkins, G. S., K. Mohr, V. R. Morris, and O. Arino, The role of convective processes over the Zaire-Congo Basin to the Southern Hemispheric ozone maximum, *J. Geophys. Res.*, *102*, 18,963–18,980, 1997.

Kaufman, Y. J., Remote sensing of direct and indirect aerosol forcing, in *Aerosol Forcing of Climate*, edited by R. J. Charlson and J. Heintzenberg, pp. 297–332, John Wiley, New York, 1995.

Kaufman, Y. J., and R. S. Fraser, Light extinction by aerosols during summer air pollution, *J. Clim. Appl. Meteorol.*, *22*, 1694–1706, 1983.

Kaufman, Y. J., A. Setzer, D. Ward, D. Tanre, B. N. Holben, P. Menzel, M. C. Pereira, and R. Rasmussen, Biomass-Burning Airborne and Spaceborne Experiment in the Amazonas (BASE-A), *J. Geophys. Res.*, *97*, 14,581–14,599, 1992.

Kaufman, Y. J., et al., Smoke, Clouds, and Radiation–Brazil (SCAR-B) experiment, *J. Geophys. Res.*, *103*, 31,783–31,808, 1998.

Kirchhoff, V. W. J. H., Y. Nakamura, E. V. A. Marinho, and M. M. Mariano, Excess ozone production in Amazon from large scale burning, *J. Atmos. Terr. Phys.*, *54*, 583–588, 1992.

Kirchhoff, V. W. J. H., J. R. Alves, F. R. da Silva, and J. Fishman, Observations of ozone concentrations in the Brazilian cerrado during the TRACE-A field expedition, *J. Geophys. Res.*, *101*, 24,029–24,042, 1996a.

Kirchhoff, V. W. J. H., P. C. Alvalá, D. L. Mauzerall, A. M. Thompson, and D. P. McNamara, Ozonesonde observations in the cerrado troposphere during SCAR-B, in *SCAR-B Proceedings*, edited by V. W. J. H. Kirchhoff, pp. 113–116, Trans Tech, Klausthal-Zellerfeld, Germany, 1996b.

Kley, D., P. J. Crutzen, H. G. J. Smit, H. Vomel, S. J. Oltmans, H. Grassl, and V. Ramanathan, Observations of near-zero ozone concentrations over the convective Pacific: Effects on air chemistry, *Science*, *277*, 230–233, 1996.

Lelieveld, J., and P. J. Crutzen, Influences of cloud, photochemical process on tropospheric ozone, *Nature*, *343*, 227–233, 1990.

Lelieveld J., and P. J. Crutzen, Role of deep cloud convection in the ozone budget of the troposphere, *Science*, *264*, 1759–1761, 1994.

Nobre, C. A., L. F. Mattos, C. P. Dereczynski, T. A. Tarazova, and I. V. Trosnikov, Overview of atmospheric conditions during the Smoke, Clouds, and Radiation–Brazil (SCAR-B) field experiment, *J. Geophys. Res.*, *103*, 31,809–31,820, 1998.

Pickering, K. E., et al., Convective transport of biomass-burning emissions over Brazil during TRACE-A, *J. Geophys. Res.*, *101*, 23,993–24,012, 1996.

Pielke, R. A., et al., A comprehensive meteorological modeling system—RAMS, *Meteorol. Atmos. Phys.*, *49*, 69–91, 1992.

Prins, E., J. M. Feltz, W. P. Menzel, and D. E. Ward, An overview of GOES 8 diurnal fire and smoke results for SCAR-B and 1995 fire season in South America, *J. Geophys. Res.*, *103*, 31,821–31,835, 1998.

Reid, J. S., P. Hobbs, R. E. Weiss, J. V. Martins, and C. Liousse, Comparisons of techniques for measuring shortwave absorption and black carbon content of aerosols from biomass burning in Brazil, *J. Geophys. Res.*, *103*, 32,031–32,040, 1998.

Silva Dias, M. A. F., and R. N. Ferreira, Application of a linear spectral model to the study of Amazonian squall lines, *J. Geophys. Res.*, *97*, 20,405–20,419, 1992.

Spinhirne, J. D., M. Z. Hanzen, and L. O. Caudill, Cloud top remote sensing by airborne lidar, *Appl. Opt.*, *22*, 1564–1571, 1982.

Stull, R. B., *An Introduction to Boundary Layer Meteorology*, *Atmos. Sci. Lib.*, Kluwer Acad., Norwell, Mass., 1988.

Thompson, A. M., Oxidants in the unpolluted marine atmosphere, in *Environmental Oxidants*, edited by J. O. Nriagu and M. S. Simmons, pp. 31–61, John Wiley, New York, 1994.

Thompson, A. M., K. E. Pickering, D. P. McNamara, M. R. Schoeberl, R. D. Hudson, J. H. Kim, E. V. Browell, V. W. J. H. Kirchhoff, and D. Nganga, Where did tropospheric ozone over southern Africa and the tropical Atlantic come from in October 1992? Insights from

TOMS, GTE/TRACE-A, and SAFARI-92, *J. Geophys. Res., 101*, 24,251–24,278, 1996.

Thompson A. M., W. K. Tao, K. E. Pickering, J. R. Scala, and J. Simpson, Tropical deep convection and ozone formation, *Bull. Am. Meteorol. Soc., 78*, 1043–1054, 1997.

Tripoli, G. J., and W. R. Cotton, The Colorado State University three-dimensional cloud/mesoscale model, I, General theoretical framework and sensitive experiments, *J. Rech. Atmos., 16*, 185–219, 1982.

Wang, Y., W.-K. Tao, K. E. Pickering, A. M. Thompson, J. S. Kain, R. F. Adler, J. Simpson, P. R. Keehn, and G. S. Lai, Mesoscale model simulations of TRACE-A and Preliminary Regional Experiment for Storm-Scale Operational Research Meteorology convective systems and associated tracer transport, *J. Geophys. Res., 101*, 24,013–24,027, 1996.

P. Artaxo, S. R. de Freitas, K. M. Longo, and M. A. Yamasoe, Instituto de Física, Universidade de São Paulo, São Paulo, Rua do Matao, travessa R, S/N, Edificio Basilio Jafet, CEP 05508-900, São Paulo-SP, Brazil. (artaxo@if.usp.br; klongo@if.usp.br)

W. Hart, L. A. Remer, J. D. Spinhirne, and A. M. Thompson, NASA Goddard Space Flight Center, Greenbelt, MD 20771. (billhart@virl.gsfc.nasa.gov; remer@climate.gsfc.nasa.gov; james.spinhirne@gsfc.nasa.gov; thompson@gsfc.nasa.gov)

V. W. J. H. Kirchhoff, Instituto Nacional de Pesquisas Espaciais, Caixa Postal 515, CEP 12201-970, São Jose dos Campos-SP, Brazil. (kir@spd.inpe.br)

M. A. F. Silva Dias, Departamento de Ciencias Atmosfericas, Instituto Astronômico e Geofisico, Universidade de São Paulo, Caixa Postal 9638, CEP 10165, São Paulo-SP, Brazil.

(Received September 17, 1997; revised October 27, 1998; accepted December 11, 1998.)